Hamburger Beiträge
zur Angewandten Mathematik

An adaptive finite element Moreau-Yosida-based solver for a coupled Cahn-Hilliard/ Navier-Stokes system

M. Hintermüller, M. Hinze, C. Kahle

Nr. 2011-18
October 2011

An adaptive finite element Moreau-Yosida-based solver for a coupled Cahn-Hilliard/Navier-Stokes system.

M. Hintermüller[a], M. Hinze[b,*], C. Kahle[b]

[a] *Humboldt-University of Berlin, Department of Mathematics, Unter den Linden 6, 10099 Berlin, Germany.*
[b] *University of Hamburg, Department of Mathematics, Bundesstrasse 55, D–20146 Hamburg, Germany.*

Abstract

An adaptive a posteriori error estimator based finite element method for the numerical solution of a coupled Cahn-Hilliard/Navier-Stokes system with a double-obstacle homogenous free (interfacial) energy density is proposed. A semi-implicit Euler scheme for the time-integration is applied which results in a system coupling a quasi-Stokes or Oseen-type problem for the fluid flow to a variational inequality for the concentration and the chemical potential according to the Cahn-Hilliard model [13]. A Moreau-Yosida regularization is employed which relaxes the constraints contained in the variational inequality and, thus, enables semi-smooth Newton solvers with locally superlinear convergence in function space. Moreover, upon discretization this yields a mesh independent method for a fixed relaxation parameter. For the finite dimensional approximation of the concentration and the chemical potential piecewise linear and globally continuous finite elements are used, and for the numerical approximation of the fluid velocity Taylor-Hood finite elements are employed. The paper ends by a report on numerical examples showing the efficiency of the new method.

Keywords: A posteriori error estimators, adaptive finite element method, Cahn-Hilliard/Navier-Stokes system, double obstacle potential, Moreau-Yosida regularization, semismooth Newton method

1. Introduction

In the present work we consider a diffuse interface model for the description of the hydrodynamics of two-phase flows, which is related to model 'H' in the nomenclatura of Hohenberg and Halperin [26]. It can be found, e.g., in [1] and reads:

*Corresponding author
Email addresses: hint@math.hu-berlin.de (M. Hintermüller), hinze@math.uni-hamburg.de (M. Hinze), christian.kahle@math.uni-hamburg.de (C. Kahle)

Find $(c(t,x), w(t,x), \mathbf{u}(t,x), p(t,x))$ such that

$$\partial_t \mathbf{u} - \tfrac{1}{Re}\Delta \mathbf{u} + \mathbf{u}\cdot\nabla\mathbf{u} + \nabla p + Kc\nabla w = 0 \quad \text{in } \Omega_T := \Omega\times(0,T), \tag{1.1}$$

$$\operatorname{div}\ \mathbf{u} = 0 \quad \text{in } \Omega_T, \tag{1.2}$$

$$\partial_t c - \tfrac{1}{Pe}\nabla\cdot(b(c)\nabla w) + \mathbf{u}\nabla c = 0 \quad \text{in } \Omega_T, \tag{1.3}$$

$$w = \Phi'(c) - \gamma^2\Delta c \quad \text{in } \Omega_T, \tag{1.4}$$

$$c(x,0) = c^0(x), \quad \mathbf{u}(x,0) = \mathbf{u}^0(x) \quad \forall x\in\Omega, \tag{1.5}$$

$$\partial_\nu c = \partial_\nu w = 0, \quad \mathbf{u} = \mathbf{g} \quad \text{on } \partial\Omega\times(0,T). \tag{1.6}$$

Here $\Omega\subset\mathbb{R}^n$, $n\in\{1,2,3\}$, is the bounded convex polygonal flow domain with boundary $\partial\Omega$ and outer unit normal ν. We note that more general domains with sufficiently smooth boundary may be used as well. The function

$$c = \frac{c_A - c_B}{c_A + c_B},$$

defined on Ω_T, denotes the concentration order parameter associated with the mass concentrations c_A and c_B in the fluid phases A and B, respectively. It satisfies $c = c(t,x)\in[-1,1]$ and $c\equiv 1$ on the pure A-phase and $c\equiv -1$ on the pure B-phase region, respectively. Initially, i.e. for $t=0$, we assume that the concentration equals c^0. The quantity w represents the chemical potential, $\mathbf{u}$ denotes the mean flow velocity field, i.e. $\mathbf{u} = \frac{1+c}{2}\mathbf{u}_A + \frac{1-c}{2}\mathbf{u}_B$, where $\mathbf{u}_A$ and $\mathbf{u}_B$ denote the fluid velocities in the fluid phases A and B, respectively, and p denotes the pressure of the fluid. The flow profile at $t=0$ is given by $\mathbf{u}^0$. The boundary values $\mathbf{g}$ have to satisfy $\mathbf{g}\cdot\nu = 0$ and in the following are assumed to satisfy $\mathbf{g}\equiv 0$. The Péclet number Pe, the Reynolds number Re and the capillary number K are given constants. The given parameter γ is related to the width of the interface region. The mobility function $b(\cdot)$ is assumed to be equal to 1 but other situations can be motivated by practical applications and are considered for example in [3]. The homogeneous free energy density is denoted by $\Phi(c)$ and in this paper it is chosen to be of double-obstacle type as proposed in [4], i.e.

$$\Phi(c) := \begin{cases} \frac{1}{2}(1-c^2) & \text{if } c\in[-1,1], \\ +\infty & \text{if } c\notin[-1,1]. \end{cases}$$

In the literature, alternative choices of the homogeneous free energy density are known with the double-well [18] and the logarithmic potential [13] being two common alternatives. Note that in contrast to the double-obstacle potential, the double-well potential allows the unphysical situation of $|c|>1$. The logarithmic potential usually prevents reaching the pure phases due to the barrier nature of the involved logarithm. When $\Phi(c)$ is chosen to be the double-obstacle potential, then (1.4) becomes

$$w + \gamma^2\Delta c \in \partial\Phi(c) \tag{1.7}$$

where $\partial\Phi$ is the subdifferential of Φ. It is well known that the potential equation (1.7) is equivalent to

$$\begin{aligned} &|c| \leq 1 \text{ a.e. in } \Omega \\ &\left\langle -\gamma^2 \Delta c - w - c, v - c \right\rangle \geq 0 \quad \forall v \in \{v \in H^1(\Omega) \,|\, |v| \leq 1 \text{ a.e. in } \Omega\} \end{aligned} \tag{1.8}$$

Here and below, 'a.e. in Ω' stands for 'almost everywhere in Ω' indicating that the associated relation holds true except on a subset of Ω which has (Lebesgue-) measure zero.

In what follows, $L^2(\Omega)$ denotes the space of measurable functions whose square is Lebesgue integrable with inner product $(\cdot\,,\cdot)$ and norm $\|\cdot\|$. By $L^2_{(0)}(\Omega) \subset L^2(\Omega)$ we denote the subspace of functions with vanishing mean value and $H^m(\Omega)$, $m \geq 1$, represents the usual Hilbert space of functions in $L^2(\Omega)$ with distributional derivatives of order less or equal m contained in $L^2(\Omega)$. The norm in $H^m(\Omega)$ is denoted by $\|\cdot\|_m$. We define $H^1_0(\Omega)$ by

$$H^1_0(\Omega) = \{v \in H^1(\Omega) \,|\, v = 0 \text{ on } \partial\Omega\},$$

where the boundary condition holds true in the sense of traces. Let $\mathbf{H}^m(\Omega) = (H^m(\Omega))^n$ and analogously for $H^m_0(\Omega)$. The dual spaces of $H^1_0(\Omega)$ and $\mathbf{H}^1_0(\Omega)$ are denoted by $H^{-1}(\Omega)$ and $\mathbf{H}^{-1}(\Omega)$, respectively. For $D \subset \Omega$ we denote by $(\cdot,\cdot)_{m,D}, \|\cdot\|_{m,D}$ and $|\cdot|_{m,D}$ the usual inner-product, the norm and the seminorm in $H^m(D)$, respectively.
Furthermore we set

$$\mathcal{V} = \{v \in H^1(\Omega) \,|\, (v,1) = 0\}$$

and

$$\mathcal{K} = \{v \in H^1(\Omega) \,|\, |v| \leq 1 \text{ a.e. in } \Omega\}.$$

For more information on Lebesgue and Sobolov spaces we refer the reader to [2].

Based on the above definitions and conventions, the variational form of (1.1)–(1.6) reads:

Find $(c(t), w(t), \mathbf{u}(t), p(t))$ in $\mathcal{K} \times H^1(\Omega) \times \mathbf{H}^1_0(\Omega) \times L^2_{(0)}(\Omega)$ such that

$$\begin{aligned}
&(\partial_t \mathbf{u}, \mathbf{v}) + \tfrac{1}{Re}(\nabla \mathbf{u} : \nabla \mathbf{v}) + B(\mathbf{u}, \mathbf{u}, \mathbf{v}) \\
&\quad -(p, \operatorname{div} \mathbf{v}) + K(c\nabla w, \mathbf{v}) = 0 && \forall \mathbf{v} \in \mathbf{H}^1_0(\Omega), \text{ a.e. in } (0,T], && (1.9)\\
&\quad (-\operatorname{div} \mathbf{u}, v) = 0 && \forall v \in L^2_{(0)}(\Omega), \text{ a.e. in } (0,T], && (1.10)\\
&\quad c(t) \in \mathcal{K} && \text{for a.e. } t \in (0,T], && (1.11)\\
&(\partial_t c, v) + \tfrac{1}{Pe}(\nabla w, \nabla v) - (c\mathbf{u}, \nabla v) = 0 && \forall v \in H^1(\Omega), \text{ a.e. in } (0,T], && (1.12)\\
&\gamma^2(\nabla c, \nabla(v-c)) - (w - c, v - c) \geq 0 && \forall v \in \mathcal{K}, \text{ a.e. in } (0,T], && (1.13)\\
&\quad c(x,0) = c^0(x) && \forall x \in \Omega, && (1.14)\\
&\quad \partial_\nu c = 0, \quad \partial_\nu w = 0 && \text{on } \partial\Omega \times (0,T], && (1.15)\\
&\quad \mathbf{u}(x,0) = \mathbf{u}^0(x) && \forall x \in \Omega, && (1.16)\\
&\quad \mathbf{u} = 0 && \text{on } \partial\Omega \times (0,T]. && (1.17)
\end{aligned}$$

Here, for $\mathbf{u}, \mathbf{v}, \mathbf{w} \in \mathbf{H}^1(\Omega)$ we use

$$B(\mathbf{u}, \mathbf{v}, \mathbf{w}) := \frac{1}{2} \int_\Omega (\mathbf{u} \cdot \nabla)\mathbf{v} \cdot \mathbf{w} \, dx - \frac{1}{2} \int_\Omega (\mathbf{u} \cdot \nabla)\mathbf{w} \cdot \mathbf{v} \, dx,$$

and

$$(\nabla \mathbf{v} : \nabla \mathbf{w}) := \int_\Omega \nabla \mathbf{v} : \nabla \mathbf{w} \, dx = \int_\Omega \sum_{i,j=1}^{n} (\nabla \mathbf{v})_{ij} (\nabla \mathbf{w})_{ij} \, dx.$$

Moreover, the initial values c^0 and $\mathbf{u}^0$ satisfy $c^0 \in \mathcal{K}$ and $\mathbf{u}^0 \in \mathbf{H}^1_0(\Omega)$.
For an analytical treatment of the above system we refer to [1, Chapter 6.5]. Especially in two space dimensions there exists a unique solution $(c, w, \mathbf{u}, p)$ to this system and we have

$$\mathbf{u} \in C^0([0,T], \mathbf{H}^1_0(\Omega)), \quad c \in BC_\omega([0,T], H^1(\Omega), \quad \nabla w \in L^2(0,T; L^2(\Omega)).$$

Here, $BC_\omega([0,T], H^1(\Omega))$ is the space of bounded and weakly continuous functions from $[0,T]$ with values in $H^1(\Omega)$.

Concerning existing literature on the development of solvers for the coupled Cahn-Hilliard/Navier-Stokes system we note here that in [29] a robust (with respect to the interfacial width; here related to γ) nonlinear multigrid method is introduced with a double-well homogeneous free energy density. We refer to [28] for the multigrid solver for the Cahn-Hilliard part only. Later, in [27] error estimates for the coupled system were derived and numerically verified. Coupled Cahn-Hilliard/Navier-Stokes systems were also considered in [8] with a double-well potential in case of three-phase flows; see also [5, 6, 7] and the references therein for further rather qualitative studies of the behavior of multiphase and mixture flows. The situation of axisymmetric immiscible two-phase flows was studied in [30] and a conservative multigrid scheme for Cahn-Hilliard fluids was developed in [31]. Concerning the numerical treatment of the sole Cahn-Hilliard system many contributions can be found in the literature. For a discussion of available solvers we refer to [21].

In this paper we are concerned with the development of a robust adaptive finite element scheme for solving the coupled Cahn-Hilliard/Navier-Stokes system with a double-obstacle homogeneous free energy density. In order to obtain a mesh independent solver, we employ a Moreau-Yosida regularization of the constraints due to the involved double-obstacle potential. Our time discretization scheme allows to solve both physical systems in separate, which, in particular, allows us to use the semi-smooth Newton iteration of [21] for the Cahn-Hilliard part (see [22] for a general account of semi-smooth Newton methods in Banach spaces). This paper, thus, extends the development contained in [21] for the Cahn-Hilliard system with a double-obstacle potential and combines it with the discretization approach to the coupled system in [27].

The rest of this paper is organized as follows. In section 2 we address the time discrete problem and establish existence of solutions for each time slice. The Moreau-Yosida regularization scheme is the subject of section 3. The finite element discretization and the a posteriori error estimation are discussed in

sections 4 and 5, respectively. Section 6 contains aspects of the numerical realization and, finally, in section 7 numerical results obtained by the new method are provided.

2. Time-discrete system

Numerically, we integrate the above system in time by using a semi-implicit Euler scheme. For this purpose, let $\tau > 0$ be the time step size. Then the values of c and $\mathbf{u}$ at $t_{\text{old}} \in [0, T-\tau]$ are denoted by $c_{\text{old}} \in H^1(\Omega)$, $\mathbf{u}_{\text{old}} \in \mathbf{H}^1_0(\Omega)$. The values of $c, w, \mathbf{u}$ and p at time $t = t_{\text{old}} + \tau$ are written as $c^\tau, w^\tau, \mathbf{u}^\tau$ and p^τ. Given $(\mathbf{u}_{\text{old}}, c_{\text{old}})$, the tupel $(c^\tau, w^\tau, \mathbf{u}^\tau, p^\tau)$ solves the problem:
Find $c \in \mathcal{K}$ and $w \in H^1(\Omega), \mathbf{u} \in \mathbf{H}^1_0(\Omega), p \in L^2_{(0)}(\Omega)$ such that

$$
\begin{aligned}
&(\mathbf{u} - \mathbf{u}_{\text{old}}, \mathbf{v}) + \tfrac{\tau}{Re}(\nabla \mathbf{u} : \nabla \mathbf{v}) + \tau B(\mathbf{u}_{\text{old}}, \mathbf{u}_{\text{old}}, \mathbf{v}) \\
&\qquad + \tau K(c \nabla w, \mathbf{v}) - \tau(p, \operatorname{div} \mathbf{v}) = 0 && \forall \mathbf{v} \in \mathbf{H}^1_0(\Omega), \quad (2.1)\\
&\qquad (-\operatorname{div} \mathbf{u}, v) = 0 && \forall v \in L^2_{(0)}(\Omega), \quad (2.2)\\
&(c, v) + \tfrac{\tau}{Pe}(\nabla w, \nabla v) = \tau(c_{\text{old}} \mathbf{u}_{\text{old}}, \nabla v) + (c_{\text{old}}, v) && \forall v \in H^1(\Omega), \quad (2.3)\\
&\gamma^2(\nabla c, \nabla(v - c)) - (w, v - c) \geq (c_{\text{old}}, v - c) && \forall v \in \mathcal{K}. \quad (2.4)
\end{aligned}
$$

In order to simplify the notation, from now on we write $c, w, \mathbf{u}, p$ instead of $c^\tau, w^\tau, \mathbf{u}^\tau, p^\tau$.

Using $v \equiv 1$ as a test function in (2.3) yields $(c, 1) = (c_{\text{old}}, 1)$ implying that the mass is conserved when solving (2.1)–(2.4).

We note that for given $\mathbf{u}_{\text{old}}$ our discretization decouples the Cahn-Hilliard equation from the Navier-Stokes system. This allows to treat (2.1)–(2.4) sequentially. First the Cahn-Hilliard part (2.3)–(2.4) is solved for (c, w) and then the Navier-Stokes part (2.1)–(2.2) is addressed with known concentration c and chemical potential w from (2.3)–(2.4). Furthermore the numerical treatment of (2.1)–(2.2) and (2.3)–(2.4) may be performed on different triangulations of the domain; see [27].

The system (2.3)–(2.4) without the concentration dependent convection term $\tau(c_{\text{old}} \mathbf{u}_{\text{old}}, \nabla v)$ is investigated in [21]. In that paper, a Moreau-Yosida regularization of the indicator function of $\mathcal{K}$ is applied. As a result, the Cahn-Hilliard variational inequality is replaced by a non-smooth equation which is then solved by a semi-smooth Newton iteration. The latter is shown to converge in the original function space setting locally at a superlinear rate. Moreover, once the function space convergence is established it may be shown similarly as in [19, 25] that the Newton solver exhibits a mesh independent convergence upon discretization on sufficiently fine meshes. In addition, for efficiency purposes, the Moreau-Yosida based semi-smooth Newton solver is intertwined with an integrated adaptive finite element method which relies on reliable and efficient residual based a posteriori error estimators. In the subsequent sections of this paper, we adapt the relevant results of [21] to the present situation of a coupled Cahn-Hilliard/Navier-Stokes system.

Before we enter the details of the Moreau-Yosida regularization, the spatial discretization and the mesh adaptation, we note that similarly to [21] it can be shown that the Cahn-Hilliard variational inequality (2.3)–(2.4) admits a unique solution. In fact, observe that (2.3)–(2.4) is related to the first order necessary and sufficient optimality condition of the problem

$$\text{minimize } \frac{\gamma^2}{2}\|\nabla c\|^2 + \frac{\tau}{2}\|\nabla w\|^2 - (c_{\text{old}}, c) \text{ over } (c, w) \in \mathcal{K} \times \mathcal{V} \tag{2.5}$$

$$\text{subject to } (c - c_{\text{old}}, v) + \frac{\tau}{Pe}(\nabla w, \nabla v) = \tau(c_{\text{old}}\mathbf{u}_{\text{old}}, \nabla v) \quad \forall v \in H^1(\Omega). \tag{2.6}$$

One readily shows that (2.5)–(2.6) admits a unique solution (c, w) with a Lagrange multiplier $q \in H^1(\Omega)$ associated with the equality constraint (2.6). The multiplier satisfies $w = q - (q, 1)$, and it can be inferred that the optimal primal-dual pair (c, q) of (2.5)–(2.6) yields the solution of (2.3)–(2.4) and vice versa.

Given (c, w) from (2.3)–(2.4), the semi-discrete Navier-Stokes system (2.1)–(2.2) admits a solution pair $(\mathbf{u}, p)$. This can be established by standard arguments for saddle point problems; see [9]. Note that p is unique only up to a constant.

3. Moreau-Yosida regularized problem

For $s > 0$, we define $\lambda_s(c) = s\,(\max(0, c-1) + \min(0, c+1))$, where the min- and max-operations are understood in the pointwise almost everywhere sense. Then $\lambda_s : \mathcal{V} \to L^2(\Omega)$ is Lipschitz continuous, $\ker(\lambda_s) = \mathcal{K}$ and λ_s is monotone, compare, e.g., [21]. Furthermore, λ_s is Newton (or slantly) differentiable (see [22]) as a mapping from $L^r(\Omega)$ to $L^2(\Omega)$ $(r > 2)$.
In the literature, also penalizations enjoying additional smoothness are considered; see e.g. [23] for a discussion on this subject and numerical implications.

The quantity λ_s is now used to replace (2.5)–(2.6) by its Moreau-Yosida regularized version. The latter notion refers to the fact that the *hard* constraint $c \in \mathcal{K}$ is replaced by a Moreau-Yosida regularization of the indicator function $I_{\mathcal{K}}$, which satisfies $I_{\mathcal{K}}(c) = 0$ if $c \in [-1, 1]$ a.e in Ω_T and $I_{\mathcal{K}}(c) = +\infty$ otherwise. The resulting regularized version of (2.5)–(2.6) reads

$$\text{minimize } \frac{\gamma^2}{2}\|\nabla c\|^2 + \frac{\tau}{2}\|\nabla w\|^2 - (c_{\text{old}}, c) + \frac{s}{2}M(c) \tag{3.1}$$

$$\text{over } (c, w) \in H^1(\Omega) \times \mathcal{V}$$

$$\text{subject to } (c - c_{\text{old}}, v) + \frac{\tau}{Pe}(\nabla w, \nabla v) = \tau(c_{\text{old}}\mathbf{u}_{\text{old}}, \nabla v) \quad \forall v \in H^1(\Omega), \tag{3.2}$$

where $M(c) = \|\max(0, c-1)\|^2 + \|\min(0, c+1)\|^2$ and the max- and min-operations are understood in the pointwise a.e. sense. Note that the Frechet-derivative M' of M satisfies $\frac{s}{2}M'(c) = \lambda_s(c)$. One readily proves existence of a unique solution (c_s, w_s) to (3.1)–(3.2), which is characterized by the first order

optimality condition

$$\left\langle F^{(1)}(c_s, w_s), v \right\rangle := (c_s - c_{\text{old}}, v) + \frac{\tau}{Pe}(\nabla w_s, \nabla v) - \tau(c_{\text{old}}\mathbf{u}_{\text{old}}, \nabla v) = 0,$$
$$\left\langle F^{(2)}(c_s, w_s), v \right\rangle := \gamma^2(\nabla c_s, \nabla v) - (w_s + c_{\text{old}}, v) + (\lambda_s(c_s), v) = 0$$

for all $v \in H^1(\Omega)$. Note that we have eliminated the adjoint state pertinent to (3.2) be means of w_s to arrive at the above first order optimality system.

As a consequence, the Moreau-Yosida regularized version of (2.1)–(2.4) is given by (compare, e.g., [21]):
Find $c_s \in H^1(\Omega), w_s \in H^1(\Omega), \mathbf{u} \in \mathbf{H}^1_0(\Omega), p \in L^2_{(0)}$ such that

$$(\mathbf{u} - \mathbf{u}_{\text{old}}, \mathbf{v}) + \frac{\tau}{Re}(\nabla \mathbf{u} : \nabla \mathbf{v}) + \tau B(\mathbf{u}_{\text{old}}, \mathbf{u}_{\text{old}}, \mathbf{v})$$
$$+\tau K(c_s \nabla w_s, \nabla \mathbf{v}) - \tau(p, \text{div } \mathbf{v}) = 0 \quad \forall \mathbf{v} \in \mathbf{H}^1_0(\Omega), \tag{3.3}$$
$$(-\text{div } \mathbf{u}, v) = 0 \quad \forall v \in L^2_{(0)}(\Omega), \tag{3.4}$$
$$\left\langle F^{(1)}(c_s, w_s), v \right\rangle = 0 \quad \forall v \in H^1(\Omega), \tag{3.5}$$
$$\left\langle F^{(2)}(c_s, w_s), v \right\rangle = 0 \quad \forall v \in H^1(\Omega). \tag{3.6}$$

Proposition 3.1. *There exists a unique solution to system* (3.3)– (3.6).

Proof. Considering slight modifications only, from [21, Theorem 4.1] it follows that for given $(c_{\text{old}}, \mathbf{u}_{\text{old}})$ (3.5)–(3.6) admits a unique solution $(c_s, w_s) \in H^1(\Omega) \times H^1(\Omega)$. Since $c_s \nabla w_s \in \mathbf{H}^{-1}(\Omega)$ using $c_s \nabla w_s$ as a volume force in (3.3)–(3.4) yields the existence of a unique $\mathbf{u} \in \mathbf{H}^1_0(\Omega)$ and a pressure $p \in L^2_{(0)}(\Omega)$ satisfying (3.3)–(3.4); see, e.g., [35].

As in [21], it can be shown that λ_s admits the Newton derivative

$$G_{\lambda_s}(c) = s\left(\chi_{\mathcal{A}^+(c)} + \chi_{\mathcal{A}^-(c)}\right)$$

satisfying

$$\|\lambda_s(c + \delta^c) - \lambda_s(c) - G_{\lambda_s}(c + \delta^c)\delta^c\| = o(\|\delta^c\|_{L^r}) \text{ as } \|\delta^c\|_{L^r} \to 0$$

with $H^1(\Omega) \subset L^r(\Omega)$ for some $r > 2$ depending on the spatial dimension and $o(\rho)/\rho \to 0$ as $\rho \to 0$. Above, χ_S denotes the characteristic function of a set $S \subset \Omega$, and we use

$$\begin{aligned} \mathcal{A}^+(c) &:= \{x \in \Omega : c(x) - 1 > 0\}, \\ \mathcal{A}^-(c) &:= \{x \in \Omega : c(x) + 1 < 0\}. \end{aligned}$$

Note that $F^{(1)}$ is Fréchet differentiable, whereas $F^{(2)}$ is only Newton differentiable due to the occurrence of λ_s. An associated Newton derivative is given by

$$\langle G_{F^{(2)}}(c, w)[\delta^c, \delta^w], v\rangle = \gamma^2(\nabla \delta^c, \nabla v) - (\delta_w, v) + (G_{\lambda_s}(c)[\delta^c], v)$$

for $(\delta^c, \delta^w) \in H^1(\Omega) \times H^1(\Omega)$ and $v \in H^1(\Omega)$.

The semismooth Newton method associated with solving (3.5)–(3.6) is specified next.

Semi-smooth Newton iteration for the Cahn-Hilliard system (3.5)–(3.6)**.**

(i) Choose $(c_0, w_0) \in H^1(\Omega) \times H^1(\Omega)$ and set $k := 0$.

(ii) Unless a stopping rule is satisfied, compute the solution (δ_k^c, δ_k^w) of

$$\begin{aligned} \langle (F^{(1)})'(c_k, w_k)[\delta_k^c, \delta_k^w], v\rangle &= -\langle F^{(1)}(c_k, w_k), v\rangle \quad \forall v \in H^1(\Omega), \\ \langle G_{F^{(2)}}(c_k, w_k)[\delta_k^c, \delta_k^w], v\rangle &= -\langle F^{(2)}(c_k, w_k), v\rangle \quad \forall v \in H^1(\Omega). \end{aligned}$$

(iii) Set $c_{k+1} := c_k + \delta_k^c$, $w_{k+1} := w_k + \delta_k^w$, $k := k + 1$, and return to (ii).

Concerning the convergence of the above iteration we have the following result.

Theorem 3.2. *The semismooth Newton iteration converges at a superlinear rate to the solution* (c_s, w_s) *of* (3.5)–(3.6) *provided that* (c_0, w_0) *is chosen sufficiently close to* (c_s, w_s).

For a proof of a result similar to Theorem 3.2 in a related context we refer to [21, Prop. 5.5]. Since the necessary modifications are rather straight forward, we refrain from displaying the proof of Theorem 3.2 here.

In our numerics we observe convergence of the Newton iteration regardless of the initial choice. In particular, we always choose $(c_0, w_0) = (c_{\text{old}}, w_{\text{old}})$. Concerning the stopping rule, we note that we stop the iteration as soon as the absolute residual of the system drops below a user specified tolerance tol_{SSN}. In our tests we use $tol_{SSN} = 10^{-6} + 10^{-12}\|(F^{(1)}(c_0, w_0), F^{(2)}(c_0, w_0))\|$.

The update of s follows the suggestion in [21], i.e., for the initial time step, starting from a rather small s value, we increase s by a factor of 10 and always use the solution of the previous s-value as the initial guess for solving the problem belonging to the next larger s-value. We note that more sophisticated update rules for s are conceivable; see [20, 24]. For the subsequent time steps, we keep s at a relatively large value and use the initialization with respect to (c, w) as explained above. The latter strategy is supported by the fact that τ is usually sufficiently small to obtain good initial guesses by considering the solution of the previous time step. Moreover, for large t the phase separation exhibits a rather slow change of the interfacial region separating the phases such that the pair $(c_{\text{old}}, w_{\text{old}})$ from the previous time step yields an excellent initial guess for solving the semi-discrete Cahn-Hilliard system in the next time step.

From here onwards our investigations are based on (3.3)–(3.6).

4. Finite element approximation

For the discretization of (3.3)–(3.6) in space we introduce shape regular simplicial meshes $\mathcal{T}^{cw}$ and $\mathcal{T}^{up}$ such that $\bar{\Omega} = \bigcup_{T \in \mathcal{T}^{cw}} T$ and $\bar{\Omega} = \bigcup_{T \in \mathcal{T}^{up}} T$.

By $\mathcal{E}^{cw}$ and $\mathcal{E}^{up}$ we denote the sets of faces associated with $\mathcal{T}^{cw}$ and $\mathcal{T}^{up}$, respectively. For a triangle $T \in \mathcal{T}^{cw}$ we denote by h_T the diameter of T and by $|T|$ its area. For a face $E \in \mathcal{E}^{cw}$ we denote by h_E the length of this face.
The concentration c and the potential w are discretized within the finite element space given by

$$\mathcal{V}_h^{cw} = \{v \in C^0(\overline{\Omega}) \,:\, v|_T \in P_1(T),\, \forall T \in \mathcal{T}^{cw}\}$$

with nodal basis $\{\phi_1, \ldots, \phi_N\}$. The velocity of the fluid $\mathbf{u}$ and the pressure p are approximated by the LBB-stable Taylor-Hood finite elements defined one $\mathcal{T}^{up}$, i.e., we set

$$\mathcal{V}_h^{u} = \{v \in C^0(\overline{\Omega}) \,:\, v|_T \in P_2(T),\, \forall T \in \mathcal{T}^{up}\},$$

and

$$\mathcal{V}_h^{p} = \{v \in C^0(\overline{\Omega}) \,:\, v|_T \in P_1(T),\, \forall T \in \mathcal{T}^{up}\};$$

see [36]. Here $P_k(T)$ stands for the space of polynomials up to degree k defined on T.

The spatially discretized version of (3.3)–(3.6) then consists in finding $(c_s^h, w_s^h) \in \mathcal{V}_h^{cw} \times \mathcal{V}_h^{cw}$ and $(\mathbf{u}^h, p^h) \in \mathcal{V}_h^{u} \times \mathcal{V}_h^{p}$ such that the following system is satisfied:

$$\begin{aligned}(\mathbf{u}^h - \mathbf{u}_{\text{old}}, \mathbf{v}^h) + \frac{\tau}{Re}(\nabla \mathbf{u}^h : \nabla \mathbf{v}^h) + \tau B(\mathbf{u}_{\text{old}}, \mathbf{u}_{\text{old}}, \mathbf{v}^h) \\ -\tau(p^h, \text{div } \mathbf{v}^h) + \tau K(c_s^h \nabla w_s^h, \mathbf{v}^h) = 0 \qquad \forall \mathbf{v}^h \in \mathcal{V}_h^u \end{aligned} \tag{4.1}$$

$$(-\text{div } \mathbf{u}^h, v^h) = 0 \qquad \forall v^h \in \mathcal{V}_h^p, \tag{4.2}$$

$$\left\langle F_h^{(1)}(c_s^h, w_s^h), v^h \right\rangle = 0 \qquad \forall v^h \in \mathcal{V}_h^{cw}, \tag{4.3}$$

$$\left\langle F_h^{(2)}(c_s^h, w_s^h), v^h \right\rangle = 0 \qquad \forall v^h \in \mathcal{V}_h^{cw}. \tag{4.4}$$

For $v \in H^1(\Omega) \cap C_0(\overline{\Omega})$ we set

$$\left\langle F_h^{(1)}(c_s^h, w_s^h), v \right\rangle := \frac{\tau}{Pe}(\nabla w_s^h, \nabla v) + (c_s^h - c_{\text{old}}, v)^h - \tau(c_{\text{old}} \mathbf{u}_{\text{old}}, \nabla v), \tag{4.5}$$

and

$$\left\langle F_h^{(2)}(c_s^h, w_s^h), v \right\rangle := \gamma^2(\nabla c_s^h,\, \nabla v) + (\lambda_s(c_s^h), v)^h - (w_s^h, v)^h - (c_{\text{old}}, v)^h, \tag{4.6}$$

where the semi-inner product $(.\,,.)^h$ on $C_0(\overline{\Omega})$ is defined via mass lumping as

$$(f, g)^h := \int_\Omega \pi^h(f(x)g(x))dx = \sum_{i=1}^{N} (1, \phi_i) f(x_i) g(x_i) \quad \forall f,\, g \in C_0(\overline{\Omega}),$$

with $\pi^h : C_0(\overline{\Omega}) \to \mathcal{V}_h^{cw}$ denoting the Lagrange interpolation operator.

Using the techniques from [21] one shows that there exists a solution to (4.3)–(4.4) which can be computed by a modified version of the semi-smooth Newton method for the semi-discrete Cahn-Hilliard system as specified above. This solution is bounded in $H^1(\Omega)$ independently of s. With (c_s^h, w_s^h) available from solving (4.3)–(4.4) and kept fixed in (4.1)–(4.2), one computes the solution $(\mathbf{u}^h, p^h)$ of the latter system, see e.g. [10, Chap. 12].

5. A posteriori error estimation

For an efficient solution of (4.3)–(4.4) we next describe an a posteriori error estimator based mesh refinement scheme. For the numerical solution of the pure Cahn-Hilliard problem such a scheme was developed in [21]. We note that the adaptation of $\mathcal{T}^{cw}$ is completely independent from a possible adaptation of $\mathcal{T}^{up}$. In our computations we use a uniform grid $\mathcal{T}^{up}$ for flow and pressure computations. Mesh adaptation is only performed on $\mathcal{T}^{cw}$ for the resolution of the concentration c and the potential w at the interface. In order to ease the notation, in what follows we drop the parameter s. Thus, $(c, w) \in H^1(\Omega) \times H^1(\Omega)$ and $(c^h, w^h) \in \mathcal{V}_h^{cw} \times \mathcal{V}_h^{cw}$ refer to the solutions of (3.5)–(3.6) and (4.3)–(4.4), respectively.

We define the following errors

$$e_c := c^h - c, \tag{5.1}$$
$$e_w := w^h - w, \tag{5.2}$$
$$e_{\lambda_s^h} := \pi_h(\lambda_s(c^h)) - \lambda_s(c^h), \tag{5.3}$$
$$e_{\lambda_s} := \lambda_s(c^h) - \lambda_s(c), \tag{5.4}$$

the residuals

$$r^{(1)} := c - c_{\text{old}} + \tau \text{div}(c_{\text{old}} \mathbf{u}_{\text{old}}), \tag{5.5}$$
$$r^{(2)} := \lambda_s(c) - w - c_{\text{old}}, \tag{5.6}$$
$$r_h^{(1)} := c^h - c_{old} + \tau \text{div}(c_{\text{old}} \mathbf{u}_{\text{old}}), \tag{5.7}$$
$$r_h^{(2)} := \pi_h(\lambda_s(c^h)) - w^h - c_{old}, \tag{5.8}$$

the element indicators

$$\eta_T^{(1)} = h_T \| r_h^{(1)} \|_{0,T} \qquad \text{for all } T \in \mathcal{T}^{cw}, \tag{5.9}$$
$$\eta_T^{(2)} = h_T \| r_h^{(2)} \|_{0,T} \qquad \text{for all } T \in \mathcal{T}^{cw}, \tag{5.10}$$
$$\eta_T^{(3)} = \| e_{\lambda_s^h} \|_{0,T} \qquad \text{for all } T \in \mathcal{T}^{cw}, \tag{5.11}$$

and the edge indicators

$$\eta_E^{(1)} = h_E^{1/2} \| [\nabla w^h]_E \cdot \boldsymbol{\nu}_E \|_{0,E} \qquad \text{for all } E \in \mathcal{E}^{cw}, \tag{5.12}$$
$$\eta_E^{(2)} = h_E^{1/2} \| [\nabla c^h]_E \cdot \boldsymbol{\nu}_E \|_{0,E} \qquad \text{for all } E \in \mathcal{E}^{cw}, \tag{5.13}$$

where, for all $E \in \mathcal{E}^{cw}$, $\boldsymbol{\nu}_E$ is the positively oriented unit normal on E.
Further, to each function $f \in L^2(\Omega)$ we assign a piecewise constant function $\overline{f}$ defined by

$$\overline{f}_{|T} = \frac{1}{|T|}(f,1)_{0,T} \qquad \text{for } T \in \mathcal{T}^{cw}.$$

The local as well as the "regional" data oscillations associated with a function f are given by

$$\mathrm{osc}_h(f,T) = \|h_T(f-\overline{f})\|_{0,T} \quad \text{for } T \in \mathcal{T}^{cw}, \tag{5.14}$$

$$\mathrm{osc}_h(f,D) = \left(\sum_{T\in D} \mathrm{osc}_h(f,T)^2\right)^{1/2} \qquad \text{for } D \subset \mathcal{T}^{cw}. \tag{5.15}$$

Next we establish reliability of our a posteriori error estimator η_Ω which is defined below. Using the above notation, the proof of this result follows the lines of the proof of Proposition 7.1 in [21].

Proposition 5.1. *There exists a constant C depending only on the domain Ω and the smallest angle of the mesh $\mathcal{T}_h^{cw}$ such that*

$$s^{-1}\|e_{\lambda_s}\|^2 + \frac{\tau}{Pe}\|\nabla e_w\|^2 + \gamma^2\|\nabla e_c\|^2 \le C\eta_\Omega^2, \tag{5.16}$$

where

$$\begin{aligned}\eta_\Omega^2 = \Big(\frac{\tau}{Pe}\Big)^{-1} \sum_{T\in\mathcal{T}^{cw}} (\eta_T^{(1)})^2 + \gamma^{-2} \sum_{T\in\mathcal{T}^{cw}} (\eta_T^{(2)})^2 + \frac{\tau}{Pe} \sum_{E\in\mathcal{E}^{cw}} (\eta_E^{(1)})^2 \\ + \gamma^2 \sum_{E\in\mathcal{E}^{cw}} (\eta_E^{(2)})^2 + \gamma^{-2} \sum_{T\in\mathcal{T}^{cw}} (\eta_T^{(3)})^2.\end{aligned} \tag{5.17}$$

Moreover

$$\eta_\Omega \le \beta(1+h^{-1})$$

with a constant β independent of s and h.

Remark 5.2.

- *The estimate* (5.16) *constitutes a reliable a posteriori error upper bound for* (4.3)–(4.4). *The term $\eta_T^{(3)}$ arises from using the finite element quantity $\pi_h(\lambda_s(c^h))$ to approximate $\lambda_s(c^h)$. Note, however, that $\eta_T^{(3)}$ contributes only in the set*

$$\mathcal{I}(c^h) := \{T \in \mathcal{T}^{cw} : \mathcal{AN}(T) \cap \mathcal{IN}(T) \neq \emptyset\} \tag{5.18}$$

of elements with a discrete active-inactive interface where the discrete inactive set is defined by

$$\mathcal{IN}(T) = \{x_i \in T : -1 < c^h(x_i) < 1\},$$

and the discrete active set is given as

$$\mathcal{AN}(T) = \{x_i \in T : c^h(x_i) < -1 \text{ or } c^h(x_i) > 1\}.$$

As a consequence of these definitions, $\eta_T^{(3)}$ *can be evaluated exactly with a rather small effort.*

- *In our numerics we assume* $div(\mathbf{u}_{old}) = 0$. *Thus, the term* $div(c_{old}\mathbf{u}_{old})$ *in* $\eta_T^{(1)}$ *reduces to* $\mathbf{u}_{old}\nabla c_{old}$.
- *Using mass-lumping only for the term* $(\lambda_s(c_s^h), v)^h$ *results in the same estimator.*

Concerning the efficiency of the residual based a posteriori error estimator, according to Proposition 7.4 in [21] we obtain the following result.

Proposition 5.3. *There exists a constant* β *depending on* s^{-1}, γ, τ, Ω, *and the smallest angle of the mesh* $\mathcal{T}_h^{cw}$ *such that*

$$s^{-1}\|e_{\lambda_s^+}\|^2 + s^{-1}\|e_{\lambda_s^-}\|^2 + \frac{\tau}{Pe}\|\nabla e_w\|^2 + \gamma^2\|\nabla e_c\|^2 \geq \beta\eta_\Omega^2 - \|e_{\lambda_s^h}\|^2 - osc_h(r_h^{(1)}, \Omega)^2 - osc_h(r_h^{(2)}, \Omega)^2. \tag{5.19}$$

The term $\|e_{\lambda_s^h}\|$ arises from the inexact evaluation of $\lambda_s(c^h)$ due to mass-lumping. If the lumping technique is replaced by an exact evaluation of $\lambda_s(c^h)$ yielding $\|e_{\lambda_s^h}\| = 0$ our estimator will be both reliable and efficient.

6. Numerical realization of mesh adaptation and the two-mesh strategy

In this section we address our implementation of the mesh adaptation for the discretization of the Cahn-Hilliard system and the realization of the joint discretization of both, the Cahn-Hilliard and the Navier-Stokes systems. The latter discretization requires a certain mesh compatibility between the adaptive Cahn-Hilliard mesh and the uniform mesh for the fluid flow.

6.1. Adaptive mesh refinement for the Cahn-Hilliard system

We now discuss the mesh adaptation strategy for $\mathcal{T}^{cw}$. The marking of elements for a possible refinement or coarsening, respectively, is based on a bulk criterion [17]. For this purpose let $\mathcal{T}^{cw}$ be a given triangulation. We introduce the set

$$\mathcal{A}_h := \{T \in \mathcal{T}^{cw} : \alpha_{\min} \leq |T| \leq \alpha_{\max}\},$$

with $0 \leq \alpha_{\min} < \alpha_{\max}$ denoting the admissible minimal and maximal element volumes, respectively. It is convenient to introduce the following indicators for

$T \in \mathcal{T}^{cw}$:

$$\eta_T = \left(\frac{\tau}{Pe}\right)^{-1} (\eta_T^{(1)})^2 + \gamma^{-2}(\eta_T^{(2)})^2,$$
$$\eta_{TE} = \sum_{E \in \mathcal{E}^{cw}(T)} \left(\frac{\tau}{Pe}(\eta_E^{(1)})^2 + \gamma^2(\eta_E^{(2)})^2\right),$$

and

$$\eta_{IA} = \gamma^{-2}(\eta_T^{(3)})^2.$$

Our mesh adaptation strategy utilizes the cycle: SOLVE–ESTIMATE–MARK–REFINE. The solver step for the Cahn-Hilliard system was addressed in the preceding sections 2-4. The semi-discrete Navier-Stokes problem results in a saddle point system and will be solved by a Krylov-subspace method as explained in section 7 below. The estimation step utilizes the error estimator derived in section 5. For the marking the following algorithm is employed.

Marking algorithm - bulk criterion.

(i) Fix constants θ^r and θ^c in $]0, 1[$.

(ii) Find a set $\mathcal{M}_h^T \subset \mathcal{T}^{cw}$ such that

$$\sum_{T \in \mathcal{M}_h^T} \eta_T \geq \theta^r \sum_{T \in \mathcal{T}^{cw}} \eta_T.$$

(iii) Find a set $\mathcal{M}_h^E \subset \mathcal{T}^{cw}$ such that

$$\sum_{T \in \mathcal{M}_h^E} \eta_{TE} \geq \theta^r \sum_{T \in \mathcal{T}^{cw}} \eta_{TE}.$$

(iv) Find a set $\mathcal{M}_h^\lambda \subset \mathcal{T}^{cw} \cap \mathcal{I}(c^h)$ such that

$$\sum_{T \in \mathcal{M}_h^\lambda} \eta_{IA} \geq \theta^r \sum_{T \in \mathcal{T}^{cw} \cap \mathcal{I}(c^h)} \eta_{IA}.$$

(v) Mark each $T \in (\mathcal{M}_h^E \cup \mathcal{M}_h^T \cup \mathcal{M}_h^\lambda) \cap \mathcal{A}_h$ for refinement.

(vi) Find the set $\mathcal{C}_h^T \subset \mathcal{T}^{cw}$ such that

$$\eta_T \leq \frac{\theta^c}{N_T} \sum_{T \in \mathcal{T}^{cw}} \eta_T$$

for each $T \in \mathcal{C}_h^T$. Here and below N_T denotes the number of elements of $\mathcal{T}^{cw}$.

(vii) Find the set $\mathcal{C}_h^E \subset \mathcal{T}^{cw}$ such that

$$\eta_{TE} \leq \frac{\theta^c}{N_T} \sum_{T \in \mathcal{T}^{cw}} \eta_{TE}$$

for each $T \in \mathcal{C}_h^E$.

(viii) Find the set $\mathcal{C}_h^\lambda \subset \mathcal{T}^{cw} \cap \mathcal{I}(c^h)$ such that

$$\eta_{IA} \leq \frac{\theta^c}{N_T} \sum_{T \in \mathcal{T}^{cw} \cap \mathcal{I}(c^h)} \eta_{IA}$$

for each $T \in \mathcal{C}_h^\lambda \cap \mathcal{I}(c^h)$.

(ix) Mark all $T \in \left(\mathcal{C}_h^T \cup \mathcal{C}_h^E \cup \mathcal{C}_h^\lambda\right) \cap \mathcal{A}_h$ for coarsening.

Note that flagging elements for refinement (resp. coarsening) is done in the three separate steps (2)-(4) (resp. (5)-(7)). This has the advantage of properly handling the scaling difference between jump, element and interpolation indicator contributions induced by τ and γ in (5.16). Observe also that the above strategy does not prevent an element T from getting marked for both refinement and coarsening. In this case the element T is refined only.

Given a mesh at a current time instance in the context of the time-dependent Cahn-Hilliard problem, we use the above marking strategy once to produce a new mesh for the next time step. This yields the following overall mesh adaptation algorithm.

Mesh adaptation scheme.

1. Determine an initial mesh $\mathcal{T}^{cw(0)}$ and an initial concentration $c^h(0)$ from c^0. Set $i := 0$.
2. Denote by t_{i+1} the current time instance and by $\mathcal{T}^{cw(i)}$ the mesh obtained from the previous time step.
3. Use $\mathcal{T}^{cw(i)}$ for solving (4.1)–(4.4) to obtain $c^h(i+1)$ and $w^h(i+1)$ as solution at the current time step.
4. For each $T \in \mathcal{T}^{cw(i)}$ calculate the above error indicators η_T, η_{TE} and η_{IA} and use them for refining or coarsening $\mathcal{T}^{cw(i)}$ to obtain $\mathcal{T}^{cw(i+1)}$.
5. Set $i := i + 1$ and go to (2).

In our numerics, this strategy performed well whenever we chose τ sufficiently small relative to the motion of the interface per time step. For resolving spinodal decomposition one is advised to choose τ sufficiently small anyway to capture the rapid dynamics at the beginning of the phase separation process. In our tests, $\tau = \mathcal{O}(\gamma^2)$ turned out to be suitable. Clearly, due to the characteristics of the time evolution in our Cahn-Hilliard/Navier-Stokes system an adaptive selection of τ or an indicator for performing more than one (spatialy) mesh adaptation cycle are of interest but go beyond the scope of this work.

6.2. Numerical realization of the two-mesh-strategy

In order to initialize the overall adaptive procedure (1)–(5) we construct the meshes $\mathcal{T}^{cw(0)}$ and $\mathcal{T}^{up}$ starting from a common macro-triangulation $\mathcal{T}^0$ of Ω for both meshes. The macro mesh is then refined to obtain $\mathcal{T}^{cw(0)}$ and $\mathcal{T}^{up}$, respectively. The mesh $\mathcal{T}^{cw(0)}$ may also be adapted to the initial concentration. The numerical solvers are then employed on the meshes resulting from this refinement procedur.

The crucial ingredient in the numerical solution of (4.1)–(4.4) is the evaluation of the terms $(c_{\text{old}}\mathbf{u}_{\text{old}}, \nabla v)$ and $(c\nabla w, \mathbf{v})$ since they contain functions defined on different meshes. In the following we describe the evaluation of $(c\nabla w, \mathbf{v})$. The evaluation of $(c_{\text{old}}\mathbf{u}_{\text{old}}, \nabla v)$ is performed similarly.

We evaluate $(c\nabla w, \mathbf{v})$ triangle-wise over all triangles of $\mathcal{T}^{up}$. On a triangle $U \in \mathcal{T}^{up}$ determine the set of all triangles $\{C_k\}_{k=1}^{n_c} \subset \mathcal{T}^{cw}$, $n_c \in \mathbb{N}$, such that $U \cap C_k \neq \emptyset$, and perform the integration on each $C_k \cap U$ exactly. The set $\{C_k\}_{k=1}^{n_c}$ can be determined easily by exploiting the fact that $\mathcal{T}^{cw}$ and $\mathcal{T}^{up}$ stem from the same macro triangulation $\mathcal{T}^0$.

In this context we invoke the following assumption.

Assumption 6.1. *There are no triangles $U \in \mathcal{T}^{up}$ and $C \in \mathcal{T}^{cw}$ such that $U \cap C \neq \emptyset$ but $U \nsubseteq C$ and $C \nsubseteq U$.*

Under this assumption exactly two situations may occur:

- The first case is $n_c = 1$ so that either $U = C_1$ or $U \subset C_1$. In both cases integration can be performed by evaluating c and w at the integration points of U.
- If $n_c > 1$, then we have $U = \bigcup_{k=1}^{n_c} C_k$. Exact integration over U is obtained by integrating exactly over each C_k and summing up for $k = 1, \ldots, n_c$.

In Figure 6.1 we show the relation of the locally adapted concentration mesh and the uniform velocity mesh. As one can see, the mesh for the concentration is locally finer than the mesh for the flow at the interface and it is locally coarser in the pure phase (bulk) regions.

We note that Assumption 6.1 is satisfied when *longest-edge bisection* is used in the refinement strategy. We also point out that the evaluation of $(c_{\text{old}}\mathbf{u}_{\text{old}}, \nabla v)$ involves three different meshes, i.e. the meshes for $c_{\text{old}}, \mathbf{u}_{\text{old}}$ and c, respectively. Among other aspects, this ensures mass-conservation of c_{old}. The latter could not be guaranteed in general if c_{old} would be extended to the mesh for c.

7. Numerical Results

In this section we report on the results obtained by our overall adaptive finite element based solver. All computations were performed on a notebook using a CPU with 1.6 Ghz and 3 GB RAM. The implementation was done in C++ based in parts on *i*FEM [14]. The linear systems arising in our semi-smooth

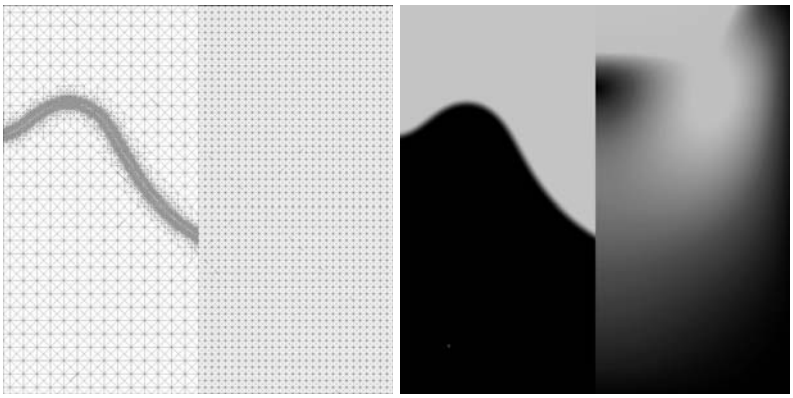

Figure 6.1: Mesh for the concentration (left plot) and flow together with the corresponding concentration and flow profile (right plot).

Newton iteration were solved by **cholmod** [15] and a LDL^t decomposition. Due to our mesh adaptation, utilizing an exact solver turned out to be feasible. In general, one may replace **cholmod** by a suitably preconditioned Krylov-subspace method; see [21] for details. For the numerical solution of the Navier-Stokes part we used a Schur complement method based on a preconditioned CG iteration with the preconditioner from [12] and an exact inversion of the Laplacian using the Cholesky decomposition from **cholmod**. For fully iterative solvers we refer to [16, 32].

Concerning the behaviour of our iterative solvers, i.e. the Newton iteration for solving the Cahn-Hillard equation and the Schur-complement method for solving the Navier-Stokes system, the Newton iteration shows the typical behaviour of an active-set method; see [22]. In fact, after a few iterations with little progress in the residual reduction at the beginning the active set is very well approximated and the system is solved to the desired accuracy within one more iteration step. In total, due to the employed direct solvers for the underlying linear systems the desired accuracy of

$$tol_{SSN} = 10^{-6} + 10^{-12}\|(F^{(1)}(c_0, w_0), F^{(2)}(c_0, w_0)\|$$

is typically reached after two or three Newton steps; except possibly for the first time instance, where a slightly larger number of Newton iterations might be required. We also tested the iterative solver proposed in [21] and still do not need more than 5 Newton steps for solving the Cahn-Hilliard/Navier-Stokes system for a given time instance to the desired accuracy.

In our settings the temporal changes in pressure and flow-field are rather small such that the quantities obtained from the old time instance are very good initial guesses for the Schur complement method. Due to the exact inversion of the Laplacian and the excellent preconditioner this method typically converges after very few steps to an absolute residual of $tol_{pcg} = 10^{-10}$.

Test problem: lid driven cavity

The first example, taken from [27], is similar to an experiment shown in [7] and is used here for validation purposes. We note, however, that in our case $b(c) = 1$ for the mobility instead of $b(c) = \exp(-c^2)$ as proposed in [27].

We set $\Omega = (0,1)^2$, $\tau = 0.0025$, $Pe = 200$, $Re = 500$, $K = 0.0002$ and $\gamma = \frac{1}{120}$. The Dirichlet boundary values are given by

$$\mathbf{g}(x) = \begin{cases} [x_1^2(1-x_1)^2, 0] & \text{if } x_2 = 1, \\ [0,0] & \text{else,} \end{cases}$$

and the initial value $\mathbf{u}^0$ for the flow is given as the solution to the steady-state Stokes problem with the boundary value $\mathbf{g}$. The initial value for c is given as a smoothed out horizontal line at $y = 0.5$, resulting in $c^0(x,y) = \tanh(100 \cdot (y - 0.5))$; see the left plot in Figure 7.1.

For c and w we use the mesh adaptation rule as described in the previous section and our initial mesh is constructed using the heuristic for adaptation as proposed in [27]. The flow velocity is obtained on a fixed mesh with uniform mesh size $h = 0.02$. Except for the mass-lumping discussed earlier, all integrations are performed exactly. For the adaption we use the parameters $\alpha_{\min} = 5 \cdot 10^{-6}$, $\alpha_{\max} = 0.01$, $\theta^r = 0.5$ and $\theta^c = 0.1$.

The numerical results obtained from our solution procedure are shown in Figure 7.1–7.4. In fact, the Figures 7.1–7.3 present the evolution of the concentration in the left plots ($c = 1$ in light gray, $c = -1$ in black and the interfacial region $-1 < c < 1$ in between) along with the associated locally adapted meshes in the right plots. Figure 7.4 displays the velocity profile in Ω at $t = 3$. Since the capillarity is very small the flow is nearly constant over the whole simulation time interval.

In Figure 7.5 we present the distribution of the error indicators η_T, η_{TE} and η_{IA} defined in section 6.1. The darker a triangle, the higher is the corresponding error indicator. One observes that the errors are primarily concentrated in and near the inactive set (interfacial region) $\mathcal{I}(c^h)$ and that the indicator η_{IA} is about 10^4 times η_T and η_{TE} which justifies the separate handling of η_T, η_{TE} and η_{IA}. Our bulk criterion for adaptation refines the interface and the triangles around it to the smallest triangle size permitted and coarsens the pure phases. For obtaining a comparable overall error magnitude when using a uniform mesh one would need 2×10^5 triangles instead of about 2×10^4 to 4×10^4 triangles in our case. The number of triangles in the adaptive context depends of course on the length of the interface, i.e. the longer the interfaces, the more triangles are to be expected. Concerning the efficiency of our adaptive concept we refer to the study in [21].

Test problem: spinodal decomposition

In our second example we investigate the spinodal decomposition of a viscous binary fluid in two space dimensions on the unit square. In this example one clearly sees the advantages of an adaptation scheme based on error estimates

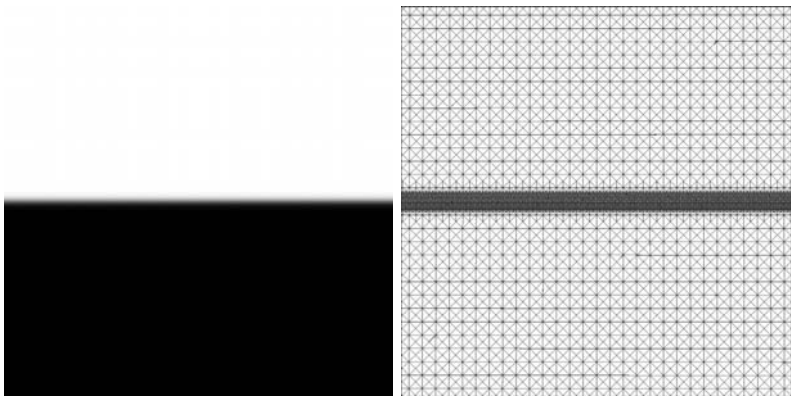

Figure 7.1: Concentration c (left) and corresponding mesh (right) at time $t = 0$.

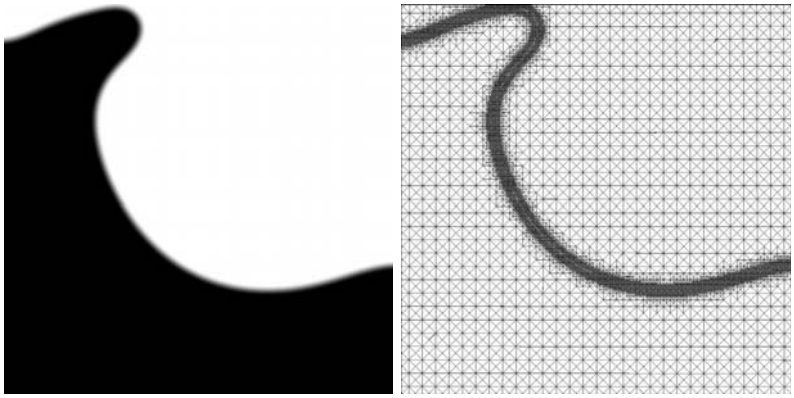

Figure 7.2: Concentration c (left) and corresponding mesh (right) at time $t = 2000\tau$.

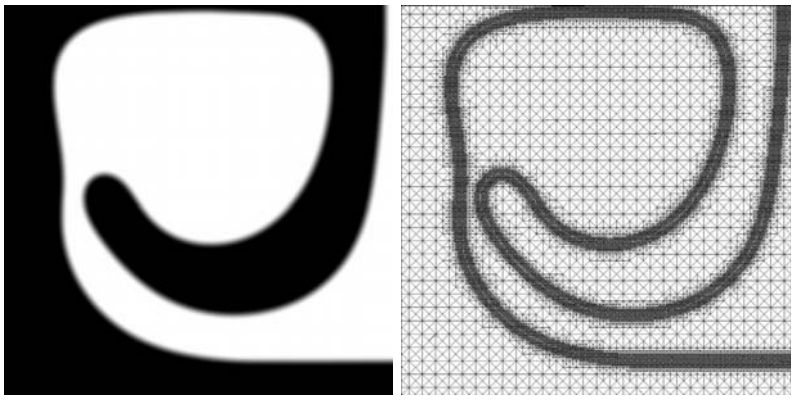

Figure 7.3: Concentration c (left) and corresponding mesh (right) at time $t = 45000\tau$.

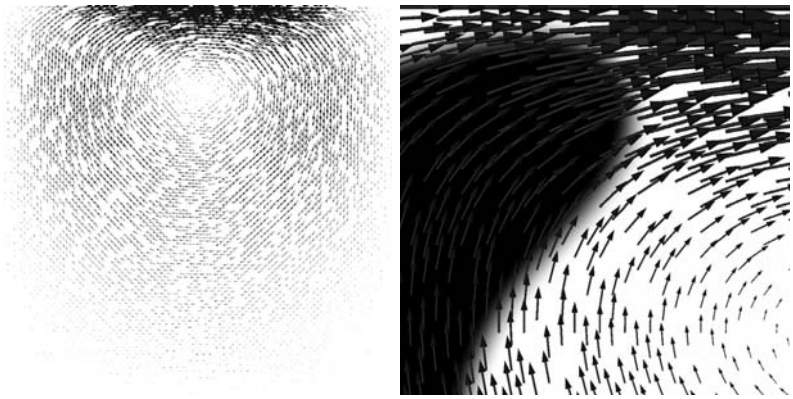

Figure 7.4: Flow profile u at $t = 2000\tau$ (left) and a zoom into the moving front (right).

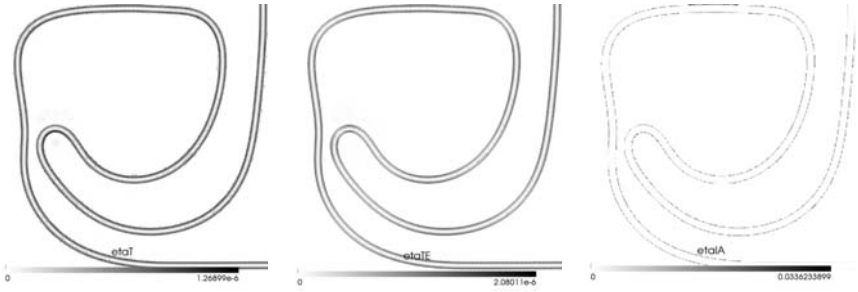

Figure 7.5: Error indicators η_T (left), η_{TE} (middle) and η_{IA} (right) for adaptation at time $t = 45000\tau$.

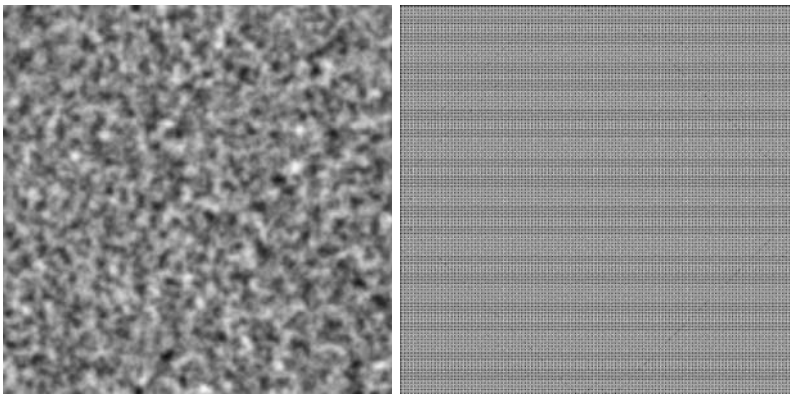

Figure 7.6: Concentration c (left) and mesh at $t = \tau$ (right).

rather than heuristics. We start the phase separation process with c^0 being white (Gaussian) noise of standard deviation 0.01 and zero mean. We choose $\tau = 5 \times 10^{-5}$, $\gamma = 1/120$ and $Pe = 1$. The flow is initialized by $\mathbf{u}^0 = 0$ on a uniform mesh with $h = 0.02$. Thus the flow field $\mathbf{u}$ is only driven by the interface. The Reynolds number is chosen to be $Re = 1$ as is the capillarity K. For the refinement cycle we use $\theta^r = 0.7$ and $\theta^c = 0.1$ together with $\alpha_{\min} = 5 \times 10^{-6}$ and $\alpha_{\max} = 0.01$.

In Figures 7.6–7.9 we show the numerical results. On the left we show the concentration variable c where again black represents -1 and white 1. On the right hand side one finds the meshes produced by our adaptive strategy. As one would expect, at the beginning of the phase separation we observe a fast evolution involving rather small-scale structures, which require a large number of triangles and nodes to be resolved well. Our residual based adaptive concept is able to cope with this effect and automatically refines to a very fine mesh. In Figure 7.11, in the left plot we show the evolution of the number of elements over the time steps (# iteration). We observe that the number of triangles peaks at the beginning and drops as time evolves. Then, as the phase separation proceeds the phase structures are coarsening yielding "pure" phases that can be resolved with only a few triangles while the interfacial region is still resolved to the maximum level (finest mesh size) permitted. In the right plot of Figure 7.11 we depict the decrease of the Ginzburg-Landau energy of the Cahn-Hilliard system over time. Due to the chosen parameters we have a diffusion dominated regime and thus we see the expected coarsening rate of $-1/3$; see [11, 34]. Note that the decrease in the number of elements follows the same rate as the free energy.

Figure 7.10 exhibits the velocity field and the pressure field at $t = 5000\tau$. Again black indicates low velocities and pressure, respectively, and white indicates high ones. Note how the pressure decreases in the interface region. For adapted finite elements for capturing this phenomenon we refer to [33].

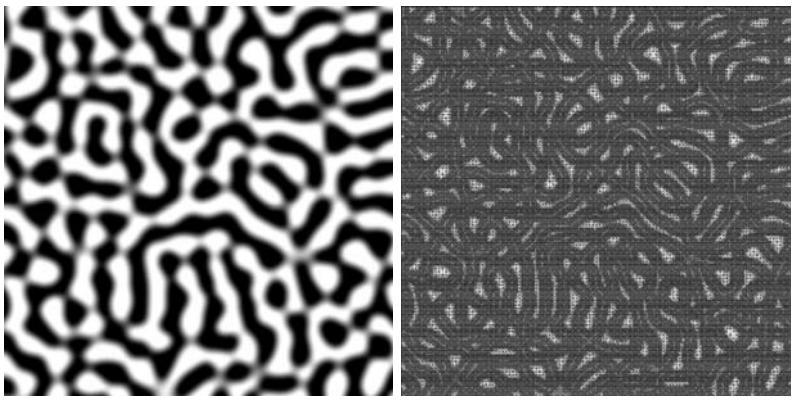

Figure 7.7: Concentration c (left) and mesh at $t = 50\tau$ (right).

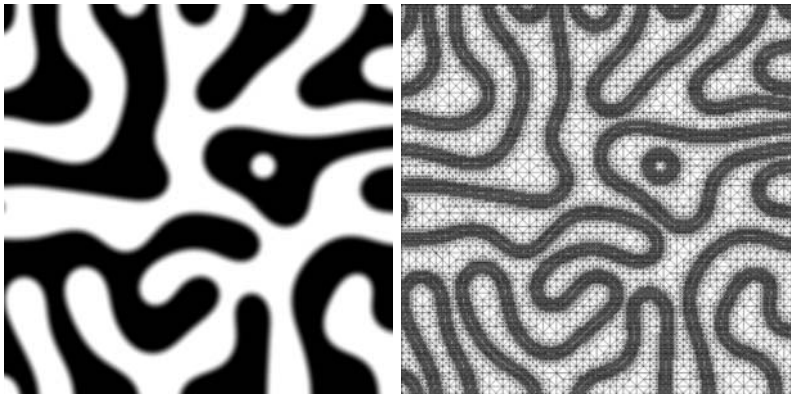

Figure 7.8: Concentration c (left) and mesh at $t = 500\tau$ (right).

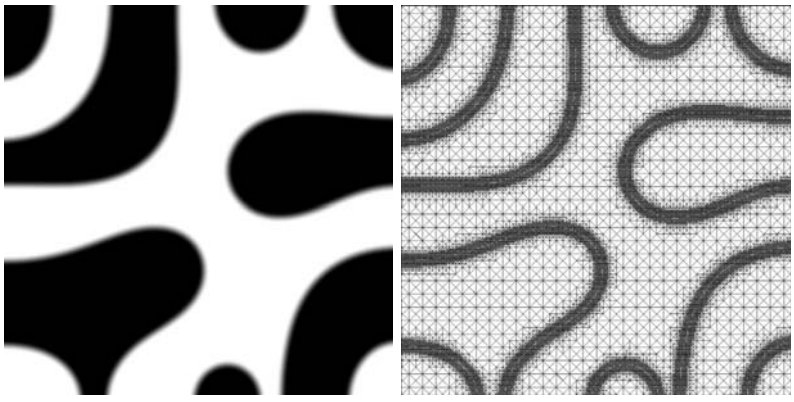

Figure 7.9: Concentration c (left) and mesh at $t = 5000\tau$ (right).

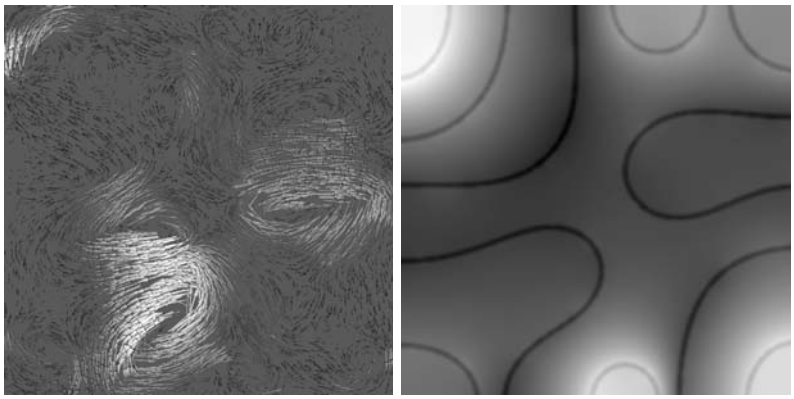

Figure 7.10: Velocity field (left) and pressure (right) at $t = 5000\tau$.

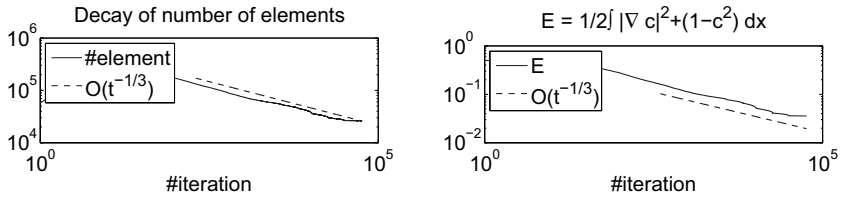

Figure 7.11: The evolution of the number of elements (left) and the Ginzburg-Landau energy E (right).

Acknowledgement

M. Hintermüller acknowledges financial support by the Austrian Ministry of Science and Research and the Austrian Science Fund FWF under START-grant Y305-N18 "Interfaces and Free Boundaries". He further acknowledges support by the German Research Fund (DFG) research center MATHEON under project C28 and C31 as well as the DFG Priority Program SPP1253 "Optimization with PDEs". M. Hinze acknowledges support by the DFG priority program SPP1253 "Optimization with PDEs".

References

[1] H. Abels. Diffuse interface models for two-phase flows of viscous incompressible fluids. *Max-Planck Institut für Mathematik in den Naturwissenschaften, Leipzig, Lecture Note no.: 36*, 2007.

[2] R.A. Adams. *Sobolov Spaces*. Pure and Applied Mathematics. Academic Press, 1975.

[3] J.W. Barrett, J.F. Blowey, and H. Garcke. Finite element approximation of the Cahn-Hilliard equation with degenerate mobility. *SIAM J. Numer. Anal.*, 37:286–318, 1999.

[4] J.F. Blowey and C.M. Elliott. The Cahn-Hilliard gradient theory for phase separation with non-smooth free energy. Part I: Mathematical analysis. *European Journal of Applied Mathematics*, 2:233–280, 1991.

[5] F. Boyer. Mathematical study of multiphase flow under shear through order parameter formulation. *Asymptotic Anal.*, 20:175–212, 1999.

[6] F. Boyer. A theoretical and numerical model for the study of incompressible mixture flows. *Comput.Fluids*, 31:41–68, 2002.

[7] F. Boyer, L. Chupin, and P. Fabrie. Numerical study of viscoelastic mixtures through a Cahn-Hilliard flow model. *European Journal of Mechanics - B/Fluids*, 23(5):759 – 780, 2004.

[8] F. Boyer, C. Lapuerta, S. Minjeaud, B. Piar, and M. Quintard. Cahn-Hilliard/Navier-Stokes model for the simulation of three-phase flows. *Transp. Porous Media*, 82(3):463–483, 2010.

[9] D. Braess. *Finite Elements*. Cambridge University Press, 3rd edition, 2007.

[10] S.C. Brenner and L.R. Scott. *The Mathematical Theory of Finite Element Methods*. Texts in Applied Mathematics. Springer, 2008.

[11] Y. Brennier, F. Otto, and C. Seis. Upper bounds on coarsening rates in demixing binary viscous liquids. *SIAM J. Math. Anal.*, 43(1):114–134, 2011.

[12] M.O. Bristeau, R. Glowinski, and J.Periaux. Numerical methods for the Navier-Stokes equations. Application to the simulation of compressible and incompressible flows. *Computer Physics Report*, 6:73–187, 1987.

[13] J.W. Cahn and J.E. Hilliard. Free energy of a nonuniform system-I: Interfacial free energy. *J. Chem. Phys.*, 28:258–267, 1958.

[14] L. Chen. *i*FEM: an innovative finite element methods package in matlab; software available at http://ifem.wordpress.com.

[15] Y. Chen, T.A. Davis, W.W. Hager, and S. Rajamanickam. Algorithm 887, cholmod, supernodal sparse cholesky factorization and update/downdate. *ACM Trans. Math. Softw.*, 35(3):1–14, 2008.

[16] H.S. Dollar, N.I.M. Gould, M. Stoll, and A.J. Wathen. Preconditioning saddle-point systems with applications in optimization. *SIAM J. Sci. Comp.*, 32(1):249–270, 2010.

[17] D. Dörfler. A convergent adaptive algorithm for poisson's equation. *SIAM J. Numer. Anal.*, 33:1106–1124, 1996.

[18] C.M. Elliott. The Cahn–Hilliard model for the kinetics of phase separation. In *Mathematical Models for Phase Change Problems*, volume 88 of *International Series of Numerical Mathematics*, pages 35–73. Birkhäuser Verlag, Basel, 1989.

[19] M. Hintermüller. Mesh-independence and fast local convergence of a primal-dual active set method for mixed control-state constrained elliptic control problems. *ANZIAM Journal*, 49(1):1–38, 2007.

[20] M. Hintermüller and M. Hinze. Moreau-Yosida regularization in state constrained elliptic control problems: Error estimates and parameter adjustment. *SIAM J. on Numerical Analysis*, 47(3):1666–1683, 2009.

[21] M. Hintermüller, M. Hinze, and M.H. Tber. An adaptive finite element Moreau-Yosida-based solver for a non-smooth Cahn-Hilliard problem. *OMS*, 2011.

[22] M. Hintermüller, K. Ito, and K. Kunisch. The primal-dual active set strategy as a semi-smooth Newton method. *SIAM J. Optimization*, 13(3):865–888, 2003.

[23] M. Hintermüller and I. Kopacka. A smooth penalty approach and a nonlinear multigrid algorithm for elliptic MPECS . *Comput. Optim. Appl.*, 50(1):111–145, 2011.

[24] M. Hintermüller and K. Kunisch. Path-following methods for a class of constrained minimization problems in function space. *SIAM J. Optimization*, 17:159–187, 2006.

[25] M. Hintermüller and M. Ulbrich. A mesh-independence result for semi-smooth Newton methods. *Math. Program.*, 101:151–184, 2004.

[26] P.C. Hohenberg and B.I. Halperin. Theory of dynamic critical phenomena. *Rev. Mod. Phys.*, 49(3):435–479, 1977.

[27] D. Kay, V. Styles, and R. Welford. Finite element approximation of a Cahn-Hilliard-Navier-Stokes system. *Interfaces and Free Boundaries*, 10(1):15–43, 2008.

[28] D. Kay and R. Welford. A multigrid finite element solver for the Cahn-Hilliard equation. *J. Comput. Phys.*, 212:288–304, 2006.

[29] D. Kay and R. Welford. Efficient numerical solution of Cahn-Hilliard-Navier-Stokes fluids in 2d. *SIAM J. on Scientific Computing*, 29(6):2241—2257, 2007.

[30] J. Kim. A diffuse-interface model for axisymmetric immiscible two-phase flow. *Appl. Math. Comput.*, 160:589–606, 2005.

[31] J. Kim, K. Kang, and J. Lowengrub. Conservative multigrid methods for Cahn-Hilliard fluids. *J. Comp. Phys.*, 193:511–543, 2004.

[32] J. Peters, V. Reichelt, and A. Reusken. Fast iterative solvers for the discrete Stokes equations. *SIAM J. Sci. Comp.*, 27(2):646–666, 2005.

[33] A. Reusken. Analysis of an extended pressure finite element space for two-phase incompressible flows. *Comp. Visual. Sci.*, 11(4-6):293–305, April 2008.

[34] E.D. Siggia. Late stages of spinodal decomposition in binary mixtures. *Phys. Rev. A*, 29(2):595–605, August 1979.

[35] R. Temam. *Navier-Stokes equations: Theory and numerical analysis.* North-Holland, Amsterdam, New York, Oxford, 3rd edition, 1984.

[36] R. Verfürth. Error estimates for a mixed finite element approximation of the Stokes equation. *RAIRO Anal. Numér.*, 18(2):175–182, 1984.